Chapter 5
Crackling Noise in Digital and Real Rocks–Implications for Forecasting Catastrophic Failure in Porous Granular Media

Ian G. Main, Ferenc Kun and Andrew F. Bell

Abstract 'Crackling noise' occurs in a wide variety of systems that respond to steady-state external forcing in an intermittent way, leading to sudden bursts of energy release similar to those heard when crumpling a piece of paper or listening to a fire. In rock physics sudden changes in internal stress associated with microscopically-brittle rupture events lead to acoustic emissions that can be recorded on the sample boundary, and used to infer the state of internal damage. Crackling noise is inherently stochastic, but the population of events often exhibits remarkably robust scaling properties, in terms of the source area, duration, energy, and in the waiting time between events. Here we describe how these scaling properties emerge and evolve spontaneously in a fully-dynamic discrete element model of sedimentary rocks subject to uniaxial compression applied at a constant strain rate. The discrete elements have structural disorder similar to that of a real rock, and this is the only source of heterogeneity. Despite the stationary strain rate applied and the lack of any time-dependent weakening processes, the results are all characterized by emergent power law distributions over a broad range of scales, in agreement with experimental observation. As deformation evolves, the scaling exponents change systematically in a way that is similar to the evolution of damage in experiments on real sedimentary rocks. The potential for real-time forecasting of catastrophic failure obeying such scaling rules is then examined by using synthetic and real data from laboratory tests and prior to volcanic eruptions. The combination of non-linearity in the constitutive rules and an irreducible stochastic component governed by the material heterogeneity and finite sampling of AE data leads to significant variations in the precision and accuracy of

I.G. Main (✉) · A.F. Bell
School of Geoscience, Grant Institute, University of Edinburgh,
James Hutton Road, Edinburgh EH9 3FE, UK
e-mail: ian.main@ed.ac.uk

A.F. Bell
e-mail: a.bell@ed.ac.uk

F. Kun
Department of Theoretical Physics, University of Debrecen, P.O. Box 5,
Debrecen 4010, Hungary
e-mail: ferenc.kun@science.unideb.hu

E.K.H. Salje et al. (eds.), *Avalanches in Functional Materials and Geophysics*,
Understanding Complex Systems, DOI 10.1007/978-3-319-45612-6_5

the forecast failure time. This leads to significant proportion of 'false alarms' (forecast too early) and 'missed events' (forecast too late), as well as an over-optimistic assessments of forecasting power and quality when the failure time is known (the 'benefit of hindsight'). The evolution becomes progressively more complex, and the forecasting power diminishes, in going from ideal synthetics to controlled laboratory tests to open natural systems at larger scales in space and time.

5.1 Introduction

There is widespread interest in the prospect of forecasting system-sized catastrophic failure events in porous media and in the Earth, from the failure of stone-built bridges to landslides, rockfalls, volcanic eruptions and earthquakes, both natural and induced. Most methods for investigating this problem rely on the recording of elastic waves on the Earth's surface or the rock sample boundary, in turn caused by much smaller earthquakes or acoustic emissions that result from locally-brittle fracture and/or shear events. Such analysis is often combined with changes in bulk properties such as stress, strain, and elastic wave velocities where available. In the Earth it is not possible to measure the stress directly – a significant handicap compared to a controlled laboratory environment. Unfortunately, the search for reliable precursors to damaging earthquakes has not so far proven fruitful despite the large literature on candidate precursors [63]. The many claimed 'precursors' can largely be attributed to the unconscious biases that are associated with retrospective selection of data containing an irreducible stochastic component ([21], see also example in [35], their Fig. 5.5). This has in turn led to modern testing programmes that require forecasting of event probability to be made publically in real time as a 'blind test', and only then evaluated in retrospect by the community (e.g. http://www.cseptesting.org/).

Many current models for such forecasting are statistical, based on empirical scaling laws for seismicity that are also features of laboratory acoustic emissions on a smaller scale. In turn they are part of a much larger family of systems exhibiting 'crackling noise', where competition between local interactions and random fluctuations in disordered media results in broad-band power-law scaling and clustering in the resultant populations of discrete avalanches or 'bursts' of energy release [53, 57].

In this paper we first introduce some of the conceptual models that have been applied to populations of brittle rupture events in Earth materials on different scales in space and time. We then describe some of the phenomenology observed in the build-up to catastrophic failure in a controlled laboratory environment, and compare these to the results of some recent numerical simulations for the emergent scaling laws in space, time and event magnitude. Modern discrete element models are shown to reproduce much of the phenomenology of acoustic emissions in real rock samples, and highlight the fundamental role of structural disorder in controlling the emergent behaviour in the population dynamics, including the evolution from spatially-random

to localised brittle failure events. Finally we assess the implications of the emergent behaviour in forecasting system-sized brittle failure events on different scales in space, time and event magnitude.

5.2 Conceptual Models for the Population Dynamics of Brittle Rupture

The population dynamics of brittle failure events is often addressed using theories derived from the analysis of phase transitions in thermodynamics and statistical mechanics. This approach has a relatively long pedigree. Griffith's theory [15, 16] for crack nucleation closely parallels Gibbs' earlier theory [14] for the nucleation of raindrops, substituting intact or broken solid as phases rather than liquid or vapour, the specific surface energy for surface tension, the strain energy held in the bulk sample for the degree of super-saturation in the cloud, and critically the degree of permanent structural disorder (pre-existing micro-cracks or flaws) for fluctuations in temperature as a source of randomly-distributed potential nucleation sites. While raindrops eventually fall out of cloud under gravity at a critical size, the original Griffith nucleation theory allows arbitrarily large or system-sized avalanches to occur when the pre-existing stable crack exceeds a critical length associated with the maximum in free energy as a function of crack size. In practice a crack nucleating in a heterogeneous medium can also be stopped by random fluctuations in strength [51]. The growing crack can also be 'blunted' by a stress shadow caused by a cloud of damage or 'process zone' occurring ahead of the crack tip [4], also associated with random strength fluctuations [52].

In more recent times the notion of phase transitions has been extended to describe the population dynamics of far-from equilibrium systems, including earthquakes and acoustic emissions, notably the statistical physics of critical point or near-critical point systems. For example, in the laboratory the mean source crack length $y = < c >$ and the cumulative number of acoustic emissions $y = N$ inferred from acoustic emission data both increase according to an inverse power law under steady-state loading conditions of constant stress or constant applied strain rate

$$y = y_0 \left(1 - \frac{x}{x_c}\right)^{-\nu} \quad , \tag{5.1}$$

where x may be strain or time, which diverges at a critical value x_c, and the exponent $\nu > 0$ [28, 29]. At the same time the scaling in the frequency-size distribution of source energy (or seismic moment - the product of the shear modulus, the rupture area and the average source displacement) take the form of a power-law with an exponential cut-off

$$N = N_o \, (E/E_0)^{-B} \, \exp\left(-\frac{E}{E^*}\right) \quad , \tag{5.2}$$

where the exponent $B > 0$, subscripts zero denote characteristic values, and E^* is a characteristic energy related to the correlation length of the population of seismic sources (approximately the size of the largest cluster of broken elements). While a finite E^* is required to maintain a finite flux of strain energy [31], it can often be difficult to pin down in natural earthquake samples due to the small samples currently available in instrumental and historical data compared to the timescales of geological processes [7, 33]. Under these conditions the frequency-distribution can be approximated as a pure power law for seismic energy or moment, or an exponential one in magnitude m – a form known as the Gutenberg–Richter law, $\log(N) = a\text{-}bm$, where a is related to the total number of events and $b = 3B/2$ [31].

Equations (5.1) and (5.2) imply that the correlation length also diverges as in (5.1). This inverse power law acceleration of the correlation length and the power-law scaling of the size distribution are both characteristic of the approach to a critical point in a variety of physical systems [11]. The analogy is complete when we regard the stress drop (related to the difference in strain energy between intact and ruptured phases) as an appropriate 'order parameter' which diminishes to zero at the critical point [34].

The systems above require tuning of an external variable to bring the system to a critical state, represented by a system-sized rupture in our case. In the Earth (and many other systems driven slowly at a constant rate of external forcing, and which release energy intermittently in discrete dynamic events or avalanches) the system instead appears *spontaneously* to have arrived at a steady state of near-critical behaviour, where the system is perpetually in a state of near failure, including locations remote from plate boundaries [1]. This state is commonly referred to as 'self-organised criticality', a relatively loose term which includes near but not precisely critical behaviour [34]. It describes the long-term averages in the system, and explains much of the phenomenology of earthquakes and faulting in a single unified theory, including the observed power-law frequency-size distribution of events, the scale-invariant or self-affine nature of observed fault structures and the ease with which earthquakes can be triggered by relatively small natural or man-made stress perturbations in the subsurface [31]. It also provides a physical basis for the assumption of long-term stationarity in time-independent probabilistic seismic hazard estimation [30].

In a state of ideal strict self-organised criticality the timing of the next system-sized event would be random and unpredictable. Such temporally-random behaviour is also an explicit assumption in time-independent seismic hazard estimation. The size of an individual event, modelled as a cascade or avalanche of neighbouring failures, is an outcome of an inherently stochastic process in the absence of detailed direct knowledge of the state of stress at each microscopic location in the Earth. The question remains 'does an earthquake know how big it is going to be when it nucleates'? The answer is that it may to some extent, in that there is a weak correlation between the rate of seismic moment released in the first few seconds and the ultimate seismic moment of earthquakes, albeit with a large scatter [13]. The moment rate function is on average front-loaded, also consistent with the stacked data shown in Fig. 5.4 of [41] and laboratory experimental data [59]. These results are consistent

with each other despite the large differences in scale, but are inconsistent with the mean field model of ([57], see their Fig. 5.7).

The large scatter between the seismic moment release soon after earthquake or fracture nucleation and its eventual total originates from the large variability in the complexity of the moment rate function [24, 57], and places significant constraints on the precision with which one could estimate an ultimate earthquake size in time to provide early warning (Kanamori, 2008). This large scatter is also consistent with rupture propagation and arrest being controlled by details of the local strength and/or dynamics that would be inaccessible to direct observation before it has occurred. Together with the absence of systematic and reliable earthquake precursors [21], this has led to a reduction in confidence in the viability of reliable and accurate deterministic earthquake prediction as a realistic scientific goal (http://www.nature.com/nature/debates/earthquake/equake_frameset.html). Nevertheless, the small but finite stress drop in the Earth allows at least in principle a degree of 'intermittent criticality' [22, 34]. Unfortunately the search for the implied acceleration to failure of the form of (5.1) has so far not passed the rigorous statistical testing needed to establish this as a general phenomenon in natural earthquake populations [17].

On the other hand purely statistical models for the probability of earthquake triggering, including aftershocks, can lead to a significant probability gain in identifying periods of transiently-elevated hazard when compared with random process, even in real time [23]. Currently the best model for such 'operational earthquake forecasting' is based on an epidemic-type point process [49], itself a variant of a more general class of self-exciting processes [19]. This model combines a random background rate with a triggering probability for consequent events which satisfies a time-reversed form of (5.1) known as the Omori law. In cases of induced or volcanic seismicity, or during earthquake 'swarms' the background rate may be non-stationary. In the Epidemic-Type Aftershock Sequence model of [49] earthquake size is randomly sampled from the scaling relation (5.2) and the triggering rate depends on a 'productivity factor' related to the triggering event magnitude (a logarithmic measure of source energy or seismic moment). The magnitude difference can be negative in rare cases due to the random sampling, leading spontaneously to occasional triggering of larger events by a smaller one. The model can be expressed mathematically in the following form:

$$\lambda(t) = \mu + A\sum\nolimits_{i,t_i<t} \exp[\alpha\,(m_i - m_C)]\left(1 + \frac{t - t_i}{c}\right)^{-p} \tag{5.3}$$

where $\lambda(t)$ is the event rate at time t, μ is the 'background' rate of independent events above a threshold magnitude m_C, c is a time constant ensuring finite event rate at $t = t_i$, p is the Omori–law exponent, α is the productivity factor for earthquake magnitude m_i, and A is an amplitude factor [49].

The model can be modified to include spatial clustering in the probability of triggering, either solely by distance or also by azimuth relative to the parent fault orientation, calculated by simulations of the immediate stress feedback and redistribution

after a large event (e.g. [40]). Longer-term 'stress renewal' models which incorporate ongoing loading and a stochastic element have also been used to estimate the effect of longer-term memory on the system, but their probability gains above a random process remain low [50].

5.3 Approach to Catastrophic Failure in a Laboratory Environment

In laboratory experiments on ceramic materials, glasses and rocks, catastrophic failure can occur below the critical stress for failure *in vacuo*, due to environmentally-assisted crack growth, even under static load. Sub-critical crack growth by thermally-activated chemical weakening processes under stress is also an intermittent, locally dynamic process that results in acoustic emissions – the macro-crack grows in jumps, and is associated with a cloud of damage associated with micro-cracks observed around the growing fracture, concentrated near the crack tip (e.g. [18]). The constitutive behaviour is often described empirically by a power law

$$V = \frac{dc}{dt} = V_0(K/K_0)^n \quad , \tag{5.4}$$

where V is velocity, K is stress intensity (a measure of stress concentration, proportional to the stress and the square root of nucleating crack length c), subscripts zero denote initial values and n is an exponent known as the 'stress corrosion index' [43]. Similar power-law behaviour can also be seen in the acoustic emission event rate dN/dt [42, 43]. This equation can be solved under conditions of constant stress to predict accelerating crack growth $c(t)$ or the total number of events $N(t)$ of the form of (5.1), with statistically-indistinguishable behaviour occurring under finite but slow stress loading conditions [32].

The intermittent and non-linear nature of quasi-static, sub-critical, crack growth is captured in the 'lattice-trapping' model, where the specific surface energy term in the Griffith nucleation theory is modulated by a sinusoid representing periodic strength variation in a crystal lattice, and the time-dependent intermittent crack growth rate is controlled by the height of the resulting local free energy barrier and hence the rate of the relevant chemical weakening reaction, modelled as a kinetic process ([27], Chap. 6). This results in a thermally-activated, intermittent crack growth even at constant stress, as well as other aspects of time-dependent behaviour such as static creep or fatigue. The theory predicts an approximately exponential dependence of V on K, but neglects the material disorder in the surrounding medium that is the origin of damage away from the crack tip, and also likely to be a fundamental control on the emergent power-law and the value of its exponent [28].

Time-dependent behaviour implies that the rate at which stress or strain is applied will affect the rheology. At high strain rates rocks produce much more brittle behaviour under compressive loading, but also more associated damage and associated

'crackling noise' in the surrounding medium that provide much more warning in the sub-critical stage. At lower strain rates (5.1) still holds, but the onset of detectable precursory acoustic emissions is delayed, the material becomes weaker (peak stress is reduced), the acceleration to failure curve becomes much sharper and the proportion of smaller events increases as the loading rate is reduced [48]. This strain-rate dependent behaviour has also been seen in other systems, including twinning avalanches occurring during high-speed impact events [53, 65].

In terms of spatial scale, the probability that one of the randomly-distributed Griffith flaws or stress concentrators being activated increases with the volume of the loaded specimen. Thus, catastrophic fracture initiates earlier for a large specimen and the macroscopically-deduced critical stress is smaller. In terms of observation and damage mechanics modelling, the material becomes both weaker and more brittle in this respect as it increases in size, behaving more like a continuum with a single flaw, as expected by the theory of Linear Elastic Fracture Mechanics [55]. Again in the limit of a very large system size, catastrophic failure would occur without warning in such a system.

On both counts we would expect predictability of individual system-sized events to degrade as the loading rate decreases and the system size increases. The logical deduction from such scaling effects is that prediction of individual earthquakes is intrinsically much harder than those of laboratory-scale fracture, and may not be possible in practical terms. This is consistent with our experience of the practical problem of deterministic earthquake prediction [23], including well-instrumented areas where a positive absence of precursors and sudden-onset rupture has been observed [2].

5.4 Squashing the Digital Rock

The above discussion has concentrated on empirical observation and models for fracture of disordered or damaged media based largely on mean-field approximations (damage mechanics), or simple cellular automaton models that capture the avalanche-like nature of the dynamics, at the expense of reducing the dimensionality of the problem to two, and the disorder to random processes acting on a geometrically-regular grid of elements (e.g. [1]). However, in critical phenomena the relevant critical exponents are known to depend to first order on the dimensionality of the model, and empirically the observed structural disorder of porous media is more amorphous than a grid. As a consequence it is necessary to tune the models to obtain the correct values of exponents such as B in (5.2), notably the dissipation factor on stress transfer after failure [34, 47].

Accordingly many researchers have turned to discrete element modelling of porous media. In the model of [25, 26]; see also [3] three-dimensional particles are represented by hard, unbreakable elastic spheres. Their diameter is selected randomly from a broad-band (log-normal) distribution, similar to that observed in a natural aquifer or hydrocarbon reservoir rock such as sandstone. The particles are

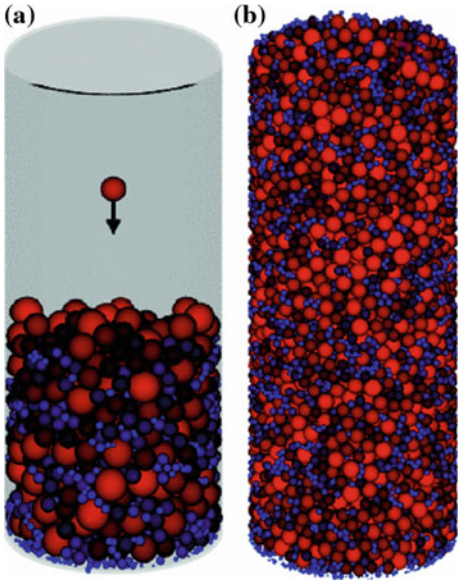

Fig. 5.1 The digital rock: **a** Illustration of its formation under sedimentation; **b** final configuration. Smaller particles are in *blue*, intermediate in *darker shades* of *red* and larger ones in *bright red* (from [25])

dropped into a cylinder under gravity, bounce around and settle in a sedimentation process that introduces a realistic structural disorder (Fig. 5.1). The particles are then cemented together by elastic bonds that can fail in either tension or torsion (shear), in both cases when the relevant stress exceeds a uniform local bond strength. The top few layers of particles are cemented by unbreakable bonds, effectively clamping the top and bottom of the sample to the boundaries where the load is applied. Some 20,000 particles were used in the above references. For a typical reservoir rock with a peak diameter at 200 microns, the equivalent bulk sample diameter is 6–7 mm. This is much smaller than the typical laboratory deformation testing range (2.5–10 cm diameter), but comparable to modern experiments aimed at elucidating the microscopic mechanisms of failure using high-resolution CT scanning using X rays [10] or neutron diffraction. At this stage of the modelling no layering or any other form of correlation above that produced by random sedimentation is introduced. This is not because we believe it to be unimportant. Instead it is because it is only with a controlled comparison with a randomly-uniform disordered medium that we could isolate the effect of such additional complexity at a later stage. The random uniform properties of the digital rock are shown in Fig. 5.2.

The digital rock is then squashed by applying a load at constant displacement rate to the upper surface of the cylinder, the lower one remaining fixed (see inset on Fig. 5.3). The combination of elastic interactions with initial structural disorder produces emergent stress heterogeneity, in the form of stress concentrations on 'force chains', and stress shadows in between. Once a bond is broken the particles are free to move dynamically and re-settle into a new configuration, arrested by the Hertzian forces acting between neighbouring spheres in contact. The Hertzian contact is the

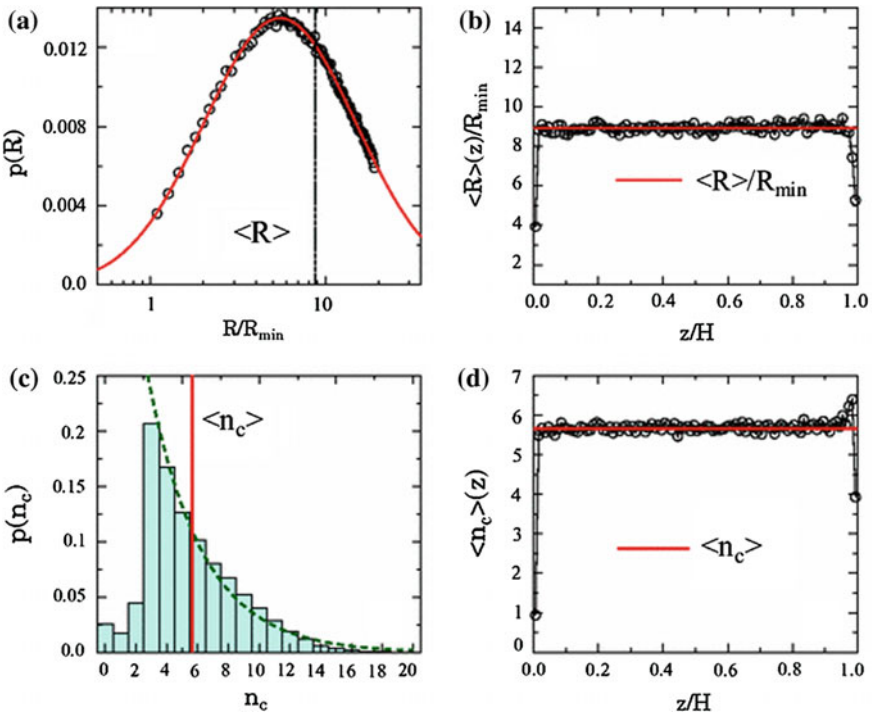

Fig. 5.2 Properties of the digital rock (from [25]). **a** Probability density function for particle radius R, normalised to its minimum value, based on sampling from a log-normal distribution. The *vertical line* indicates the average value <R>. **b** Variability of <R> as a function of vertical position z, normalized to the cylinder height H. **c** Probability density function for the number of contacts each particle has with its neighbours n_c. The *vertical red line* shows the average $< n_c >$ or 'co-ordination number'. **d** Co-ordination number as a function of z/H

basis for emergent frictional behaviour at the macroscopic level [56]. The broken bonds do not heal, and stress is redistributed dynamically to the neighbouring bonds, producing avalanches or cascades of bond ruptures representing correlated 'bursts' of energy release. While elastic radiation does take place, there is no need to put model transducers on the digital rock boundary and infer the source parameters. Instead parameters such as event time, hypocentre location, source energy, rupture area (or the number of broken bonds Δ as a proxy), average slip, the related seismic moment (product of shear modulus, rupture area and average slip), inter-event time can all be calculated directly from the model. The collective properties of this population are then a direct analogue for the source parameters of the 'crackling noise' observed in real rock samples during a laboratory test, with the advantage of having a complete sample of all local failure events.

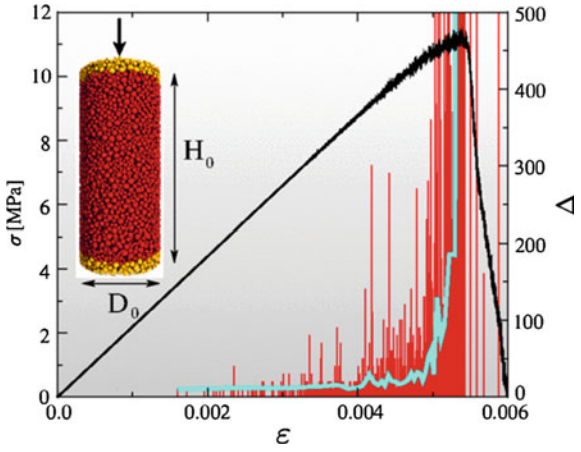

Fig. 5.3 Squashing the digital rock. The inset shows the digital rock, diameter D_0 and Height H_0, with the *top* few infinitely strong layers highlighted in *yellow*, and the direction of uniaxial force as an arrow. The *black curve* shows the stress σ as a function of strain ε, the *vertical red lines* represent the rupture area proxy Δ for each event, and the *blue line* the average $< \Delta >$ (from [26])

5.5 Properties of the Crackling Noise

The event sizes Δ are also shown in Fig. 5.3, both as a 'comb' plot of discrete individual events and as a running average. Crackling noise starts early – well before any sign of non-linearity in the stress-strain curve, and the mean event size accelerates rapidly after the yield point, in a manner similar to (5.1). The frequency-size distribution has the same form as (5.2) over a broad range of length scales in Fig. 5.4. As deformation progresses the best fit power-law exponent decreases (the slope becomes flatter) and the implied correlation length (related to the largest rupture size) increases. System-sized failure near the critical strain ε_c is marked by large apparent outlier events from the trend in (5.2) often termed 'dragon kings' [58] or, for natural seismicity, 'characteristic earthquakes'. Such a large gap between the largest and the next largest correlated cluster of broken bonds, allied with the large stress drop, is more reminiscent of a first order phase transition. However, establishing such 'dragon kings' are meaningful statistical outliers in natural data is often very difficult [45].

The event locations are dominated by the random disorder initially (see locations of nucleation points illustrated in Fig. 5.4), but increasingly localise on an incipient fault plane [25], just as occurs in experimental data on sandstone [28]. At the same time the correlation function of nucleation points spontaneously tends to a power law, with a power-law exponent (correlation dimension) decreasing to $D_2 = 2.25$ near the failure time [25]. This behaviour is in good quantitative agreement with the results of laboratory acoustic emission locations, where similar to the range observed in laboratory tests where D_2 starts off at around 2.75 when the deformation is more randomly distributed, and then decreases to around 2.25 near the failure time [20]. At the same time the incremental frequency-rupture area exponent (for the range of events shown) decreases from 1.1 to 0.4 (Fig. 5.4).

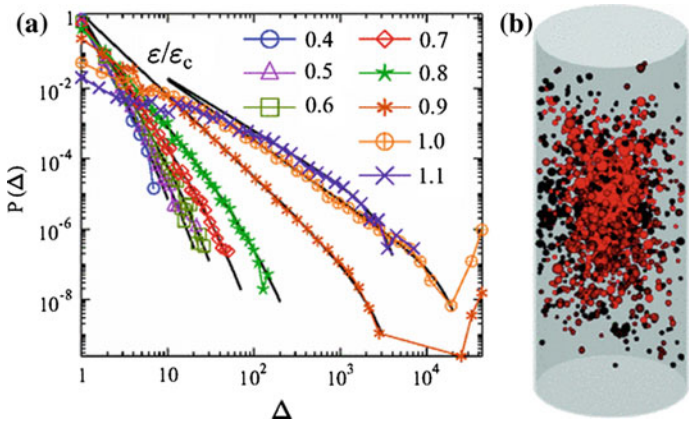

Fig. 5.4 The *left-hand* diagram shows the evolution of the probability density function for source size $p(\Delta)$, split up into consecutive increments of normalised strain indicated by the event numbers shown. The diagram on the *right plots* the location of the nucleation points for dynamic rupture cascades, an analogue for the location of acoustic emission sources

Figure 5.5 compares the results of the discrete element model with those of a laboratory test on natural sandstone. The mean event size for the digital rock increases in a similar way to that expected from combining (5.1) and (5.2), and the real data for event rate follow (5.1) directly, i.e. both are inverse power laws. The exponent ξ of the probability density function $p(\Delta)$ decreases monotonically in the model from around 4 to 1.5. The Gutenberg–Richter 'b-value' shown for the real data is defined by the slope of the cumulative or incremental frequency curve for event magnitude, itself a logarithmic measure of energy. For a sensor acting as a velocity transducer and a constant stress drop model for acoustic emission sources, the b-value is related to B in (5.2) by $b = 3B/2$ with $E \sim A^{1.5}$ and $p(A) \sim A^{-b-1}$ (e.g. [31]). Assuming rupture area scales linearly with the number of broken bonds, $A \sim \Delta$, the values of ξ imply a b-value decreasing from around 3 to 0.5 as failure approaches. This compares with the observation on Fig. 5.4 that $1.5 < b < 0.5$ in the laboratory tests. The absence of higher b-values early in the loading cycle in the laboratory tests could be due to a break down in the scale-independent stress drop model, or to data censoring of smaller events below ambient noise levels. Nevertheless, the inferred b-values for the later part of the real and laboratory tests are quantitatively similar, and exactly the same (around 0.5) immediately prior to catastrophic failure. A b-value prior to catastrophic failure of around half of the long-term average is also consistent with values reported for earthquake foreshocks, in cases where they are observed after the fact [44].

For the digital rock, the scaling may not be strictly self-similar. The energy of the bursts E scales with Δ as $E \sim \Delta^{1.15}$ [26]. This may be because the scaling of slip to rupture area is self-affine (power-law of slope less than 0.5) rather than self-similar, and/or because the parameter Δ (the number of broken bonds) does not scale

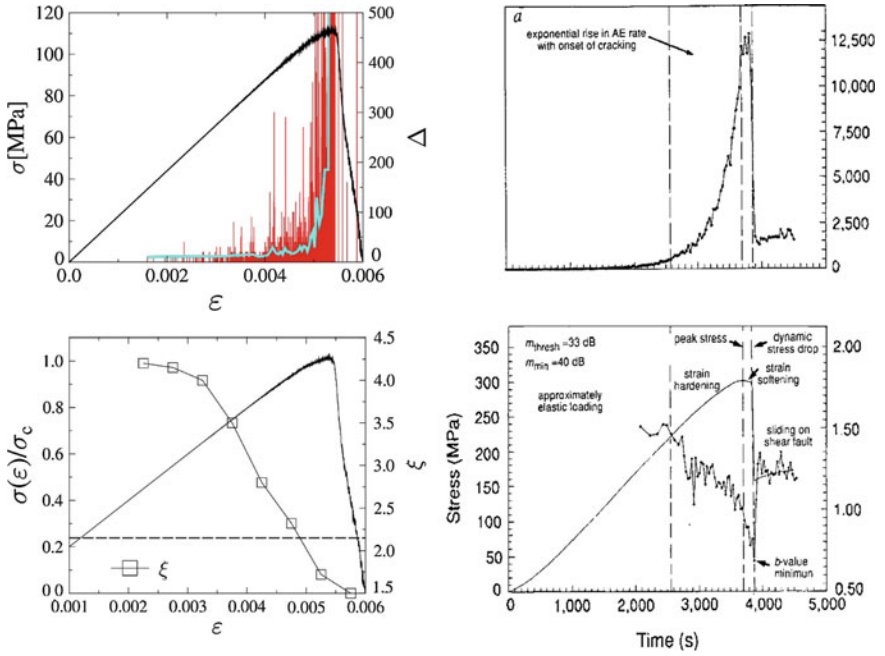

Fig. 5.5 Comparison of the model simulation results (*left hand* column, replotted after [25, 26]) with a real dry rock (*right-hand* column, from [54]). The *upper* diagrams show the acceleration of event size for the model (as in Fig. 5.3) compared to the event rate data (*top right* diagram). The *lower left* diagram show the power-law exponent of the probability density function for source size Δ (one curve for a constant strain window as in Fig. 5.4, and one for a constant number of events in each sub-sample) compared to the seismic *b*-value evolution in a laboratory test

linearly with rupture area A. If we assume instead that magnitude is a logarithmic function of energy, then the observed scaling range for ξ implies that the exponent B for the energy distribution ranges from 2.9 to 0.37 or so, or an implied b-value range for a scale-independent stress drop model of $4.3 < b < 0.55$, i.e. a slightly wider range for the early part of the loading cycle but a similar value immediately prior to system-sized failure.

After catastrophic failure the digital rock is broken in two main intact blocks, separated by a fault that takes the form of a deformation band of broken fragments - as observed in laboratory tests (Fig. 5.6). The deformation band contains a fault 'gouge' of fragments or isolated original particles with a broad bandwidth of sizes – with large fragments floating in a ground mass of smaller ones. There is significant damage (local micro-fractures) in the zone around the main fault, and a complex three-dimensional rugged geometry of the fault walls, with variable fault thickness along the fault trace. The probability density function for particle mass in the digital rock deformation band for particles containing at least two elements has the same form as (5.2) with a power law exponent $\tau = 2.1$ over two orders of magnitude [26],

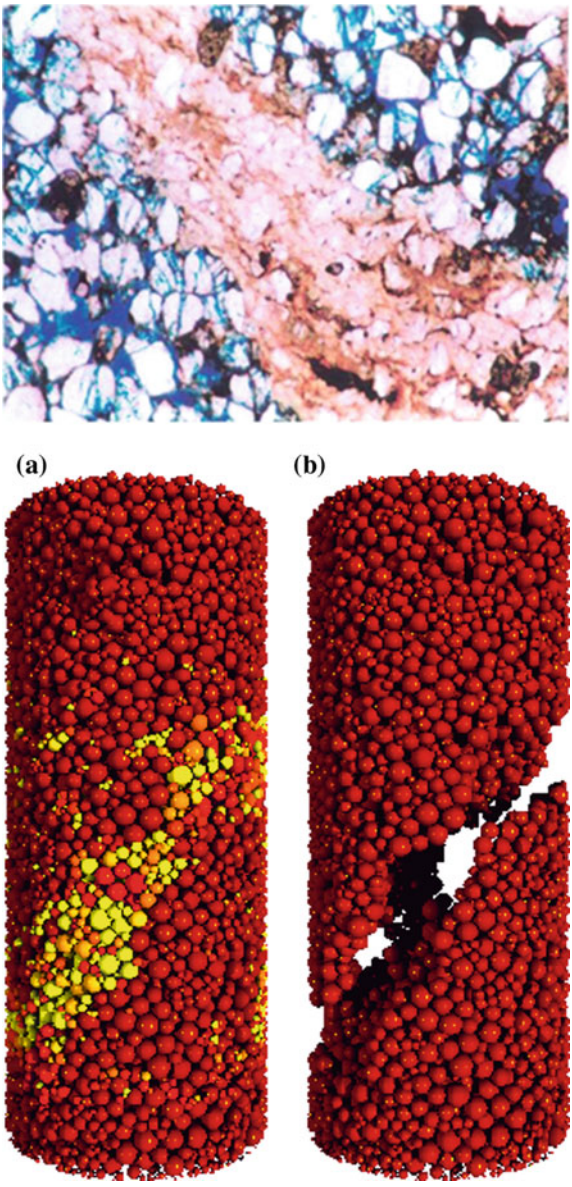

Fig. 5.6 Post-failure structure. The *upper* diagram shows a photo-micrograph of a thin section of a deformed laboratory sample of sandstone (colour version of the diagram shown in [37]). The rock has been injected with a fluorescent-dyed epoxy resin to preserve the structure and highlight locations of fracturing in *blue*. The lower diagram shows the digital rock after dynamic failure (from [25]): **a** The broken elements are shown in *yellow*, and the intact in *red*. **b** Image with broken elements removed

or (for the spherical particles of the discrete element model) an implied power-law exponent for the incremental frequency of particle diameter of $D = 3.3$. For real rocks the exponent of the frequency-particle length distribution for tests similar to those that produced the thin section in Fig. 5.6 (from [36], their Fig. 4.15), and those of real fault gouges (e.g. Table 3.1 of [61]) is $D \approx 2.6$. The main differences are likely

to be due to the angularity of the fragments in the real rock, the unbreakable nature of the discrete elements in the digital rock, and the lack of a confining pressure in the digital rock simulations. These remain a computational challenge that is currently being addressed in fully 3D simulations [38].

Emergent power laws of the form of (5.2) are also observed in the probability density functions for energy $p(E)$, duration $p(T)$, and waiting time between events $p(t_w)$ in the period before peak stress ([26], their Fig. 5.3). The distributions for energy and duration both show evidence of roll-offs in probability for smaller values associated with a lower cut-off to scale-invariant behaviour, whereas the source area proxy distribution $p(\Delta)$ does not. Best fits were obtained with the power-law exponents $\alpha = 2.02$, $\beta = 2.4$ and $z = 2.0$ for the probability density function of burst energy, duration and waiting time respectively, averaged over the period prior to the peak stress. This compares to an implied $\alpha = 1.67$ for an average $b = 1$ in the laboratory test of Fig. 5.5, and to $\alpha = 1.40 \pm 0.05$ for the uniaxial compression experiments of Vycor, a synthetic silica ceramic of ~40 % porosity [5].

The exponent for the waiting time distribution prior to peak stress in our numerical model $z = 2$ is significantly higher than that found by [5] with $z = 0.93 \pm 0.05$ for most of the time range of their laboratory tests. This discrepancy is most likely due to the absence of time-dependence in the properties of the digital rock at this stage of the modelling. References [5, 60] showed that a power-law inter-event time can be explained as an emergent property of the distribution of background and 'aftershock' events, based on the epidemic-type aftershock sequence (ETAS) model for earthquake populations. Even without aftershocks or more generally triggered events, a power law scaling in the inter-event time probability distribution can result from a non-stationary linear increase in the rate of independent events [64]. The lack of time dependence in our model means the properties of the digital rock do not depend on the loading rate, also in contrast to that seen in laboratory experiments [48], and would not result in long term creep and fatigue – another limitation compared to real rocks and other kinds of porous media. Despite these caveats, the similarity between the behaviour of the digital rock and laboratory samples, as well as the scaling to the properties of the Earth's crust are quite remarkable.

5.6 Implications for Forecasting

There are a number of clues to when catastrophic failure might occur, both in the models and in the observations collected in laboratory tests described above. These include event rate accelerating towards a singularity according to (5.1), reducing b-value, increased localisation of events in space along an incipient fault plane, and systematic changes to other exponents. In the laboratory or the digital rock a visual yield point is clear and the peak stress is a strong indicator of the onset of the final approach to failure. In the limit of an extremely brittle material catastrophic failure does occur at peak stress, but for many porous rocks system–sized failure occurs at a critical strain significantly beyond the peak stress, as captured in Fig. 5.5.

The most accurate failure forecasting model will then involve a combination of these metrics. This may be with a physical model (that also accounts for stochastic fluctuations), or a statistical approximation that may have more Information content (equally good fit with fewer free parameters). In practical scenarios there may be insufficient data for such a rigorous approach due to lack of data. For example practical volcano forecasting is often done using Bayesian 'event trees', where event rate and *b*-value changes can be included formally, along with other more subjective, 'expert' knowledge [39].

Let us now consider an ideal case, where the underlying AE rate accelerates to the critical point according to (1) plus or minus random fluctuations associated with material heterogeneity and/or finite sampling (counting errors). This defines the absolute limits of predictability of such an approach in an ideal case. By running several Monte-Carlo realisations [6, 8] mapped out the systematic and random errors involved in fitting (5.1) to infer the forecast failure time and its uncertainty for this case. To simulate a real-time or prospective forecast scenario they performed the inference at different times prior to the pre-determined failure time. First they showed that linearized versions of (5.1), often used for example in analysing seismicity associated with volcanic eruptions, introduce a systematic bias to the forecast failure time, even when data including the failure time are used. Instead a fully non-linear maximum likelihood fit to (1), assuming an underlying non-stationary Poisson process, produces a less biased fit. The random or statistical uncertainties are initially very large, and reduce significantly as more data are collected, and the most accurate forecast is after the system-sized event has occurred. This highlights the practical difficulties in evaluation of the significance of precursors retrospectively as descried by [21].

In evaluating such behaviour it is also critical to test competing hypotheses for the underlying behaviour of the time series. Accordingly [8] tested (i) stationary, (ii) exponential acceleration and (iii) (5.1) models concurrently, selecting the preferred model using a Bayesian Information Criterion, a modern form of Ockham's razor that accounts for the balance between the model residuals and the number of free parameters. A precursor is detected when the stationary model can be rejected, and a system-sized failure time cannot be defined unequivocally until (5.1) is the preferred model. The results showed that it is relatively easy to define a precursor, but an unequivocal failure time cannot be determined until relatively late in the cycle. Therefore it is possible to identify periods of enhanced probability of failure, but the precise failure time may not be known until very near or after the fact.

In real volcanic earthquake data the acceleration (determined after the fact) can be more complex that (5.1), leading to systematic errors in the best fit eruption time [7]. Such real data shows that accelerating sequences most often end in intrusions, where magma freezes in place underground rather than being extruded in eruptions [12]. Unfortunately the statistics of these two processes cannot currently be distinguished, so it is not possible to discriminate between them in real time unambiguously. This implies that local Civil Protection authorities would then have to live with many 'false alarms'. In real volcanic data (1) can be a good fit, but often the exponential model is preferred throughout or until just before the failure time. This limits the possibility of

a successful planned and orderly evacuation based on such a deterministic forecast. In this case there may be many 'misses' when the forecast time is after the eruption time, as well as 'hits' when the two are the same within the extrapolated uncertainty. Over time the ratio of 'hits', 'misses' and 'false alarms' will help quantify the hazard and risk probabilities, and also help educate the public on the practical limits of what science can do in forecasting such a complex, non-linear system [9]. Nevertheless, this probabilistic, risk-based approach has achieved some remarkable successes, leading to successful evacuations at the right time, for example at Mount St Helens, US, in 1980 and at Pinatubo, Philippines, in 1991.

5.7 Influence of Material Heterogeneity on Forecasting Power

The Griffith theory highlighted the important role of heterogeneity due to initial flaws (cracks and/or pores) in the fracture process of an otherwise intact material. Accordingly it would not be surprising if material heterogeneity would have a significant effect on the forecasting power. To test this notion Vasseur et al. [62] generate a suite of synthetic samples porous silicate liquids undergoing the glass transition with variable heterogeneity. A heterogeneity (disorder) parameter is defined by $H = \varphi - 0.5$, where φ is the porosity, such that $H = 0$ when φ=0 (perfect order) and $H = 1$ when φ=0.5 (perfect disorder). These synthetic porous media consisted of a range of samples of the same material, but with different porosity and microstructure (see their Fig. 5.1), in turn controlled by the gas volume fraction held in the cell during their synthesis. They then placed the synthetic rock under uniaxial compression, and recorded the AE generated in the approach to catastrophic failure.

In analysing the data (Fig. 5.7, from [62]) the exponential model is preferred when H is low, and the inverse power law when the degree of heterogeneity is high, as anticipated by the fibre bundle model of [46]. If a best-fit inverse power law is forced, then its prediction error (the normalised difference between the estimated failure time and the actual one) decreases significantly with the increasing material heterogeneity. In this sense catastrophic failure is easier to predict in heterogeneous materials. The material with high H has fewer events (Fig. 5.7a) most likely because of a greater proportion of 'silent' damage due to elastic pore closure as porosity increases. This variability in behaviour as a function of the degree of material heterogeneity may explain the large variability observed in real systems, and in time may improve the reliability and accuracy of operational forecasts, if it can be used to constrain the forecasting power in different settings.

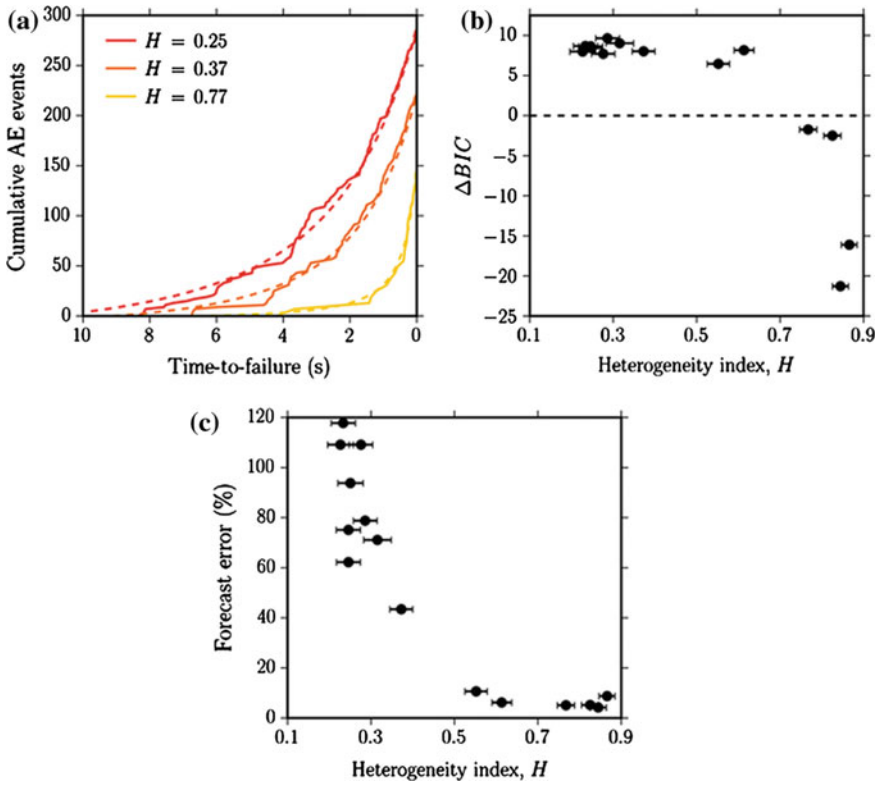

Fig. 5.7 Test of forecasting power as a function of the heterogeneity index $H = \phi - 0.5$, where ϕ is the porosity (from [62]). **a** Cumulative AE events (*solid lines*) and their maximum-likelihood best-fit curves (*dashed lines*). **b** Model selection using the difference in the Bayesian Information Criterion ΔBIC between exponential and inverse power-law acceleration in **(a)** The inverse power law is preferred when $\Delta\text{BIC} < 0$. **c** Heterogeneity-dependence of the forecast error, defined as the absolute difference between the predicted failure time and the experimental failure time, normalised by the deformation time, expressed as a percentage

5.8 Conclusion

A discrete element model with a particle size distribution similar to that of porous sandstone can now reproduce many of the scaling relationships observed in crackling noise in real rocks with similar properties. Despite the stationary loading rate and the lack of any time-dependent weakening processes, the results are all characterized by emergent power law distributions over a broad range of scales, in quantitative as well as qualitative agreement with experimental observation. As deformation evolves, the scaling exponents change systematically in a way that is similar to the evolution of damage in experiments on real sedimentary rocks. The combination of non-linearity in the constitutive rules and an irreducible stochastic component governed by the

material heterogeneity and finite sampling of AE data leads to significant variations in the precision and accuracy of the forecast failure time using constitutive rules derived from the model. The evolution of the crackling noise becomes progressively more complex, and the forecasting power diminishes, in going from the ideal behaviour revealed by the discrete element model to controlled laboratory tests to open natural systems at larger scales in space and time. Material heterogeneity plays a significant part in the emergent power-law scaling, and also affects the forecasting power. The results imply significant forecasting power above a random process that could be used in operational forecasting scenarios involving non-stationary seismicity, including seismicity induced by subsurface engineering projects and by magmatic processes leading up to volcanic eruptions.

Acknowledgments The bulk of this paper is based on the Néel lecture delivered by IGM at the 2014 European Union of Geosciences meeting in Vienna, and a shortened version delivered to the 'Avalanches in Functional Materials and Geophysics' meeting in Cambridge the same year. FK and AFB made significant material contributions to the presentations, and to the writing of this paper. IGM is grateful to Philip Meredith for many insights into rock physics that motivated the work described in the paper, as well as the many co-authors cited in the reference list, especially Jeremie Vasseur whose experimental results are reproduced in Fig. 5.7. Much of the work described in this paper was supported by the European Commission via the Complexity-NET pilot project 'LOCAT' and by the NERC project 'EFFORT', NE/H02297X/1.

References

1. P. Bak, C. Tang, Earthquakes as a self-organised critical phenomenon. J. Geophys. Res. **94**, 15635–15637 (1989)
2. W.H. Bakun et al., Implications for prediction and hazard assessment from the 2004 Parkfield earthquake. Nature **437**, 969–974 (2005). doi:10.1038/nature04067
3. P. Ball, How rocks break. Physics **7**, 16 (2014)
4. G.I. Barenblatt, The mathematical theory of equilibrium cracks in brittle fracture. Adv. Appl. Mech. **7**, 55 (1962)
5. J. Baró, Á. Corral, X. Illa, A. Planes, E.K.H. Salje, W. Schranz, D.E. Soto-Parra, E. Vives, Statistical similarity between the compression of a porous material and earthquakes. Phys. Rev. Lett. **110**, 088702 (2013)
6. A.F. Bell, M. Naylor, M.J. Heap, I.G. Main, Forecasting volcanic eruptions and other material failure phenomena: An evaluation of the failure forecast method. Geophys. Res. Lett. **38**, L15304 (2011). doi:10.1029/2011GL048155
7. A.F. Bell, M. Naylor, I.G. Main, Convergence of the frequency-size distribution of global earthquakes. Geophys. Res. Lett. **40**, 2585–2589 (2013a). doi:10.1002/grl.50416
8. A.F. Bell, M. Naylor, I.G. Main, The limits of predictability of volcanic eruptions from accelerating rates of earthquakes. Geophys. J. Int., (2013b), doi:10.1093/gji/ggt191
9. A.F. Bell, C.R.J. Kilburn, I.G. Main, Volcanic eruptions: real-time forecasting, in *Encyclopedia of Earthquake Engineering*, ed. by M. Beer, E. Patelli, I. Kougioumtzoglou, S.-K. Au (Springer, Berlin, 2015). doi:10.1007/978-3-642-36197-5_43-1
10. P. Bésuelle, G. Viggiani, N. Lenoir, J. Desrues, M. Bornert, X-ray micro CT for studying strain localization in clay rocks under triaxial compression. J. Strain Anal. Eng. Des. **40**(2), 185–197 (2006)
11. A., Bruce, D. Wallace, Critical point phenomena: universal physics at large lengthy scales, in Davies, P. (ed.) (The New Physics, Cambridge, 1989), p. 516

12. S.F.M. Chastin, I.G. Main, Statistical analysis of daily seismic event rate as a precursor to volcanic eruptions. Geophys. Res. Lett. **30**(13), 1671 (2003). doi:10.1029/2003GL016900
13. S. Colombelli, A. Zollo, G. Festa, M. Picozzi, Evidence for a difference in rupture initiation between small and large earthquakes. Nat. Commun. **5**, 3958 (2014). doi:10.1038/ncomms4958
14. J.W. Gibbs, *Elementare Grundlagen der Statistischen Mechanik* (Johann Ambrosius Barth, Leipzig, 1905)
15. A.A. Griffith, The phenomena of rupture and flow in solids. Phil. Trans. Roy. Soc. Lond. A **221**, 163 (1920)
16. A.A. Griffith, The theory of rupture,, ed. by C.B. Biezzo, J.M. Burgers, J. Waltman Jr., Proceedings of the First International Congress on Applied Mechanics, (Delft, 1924), p. 55
17. J.L. Hardebeck, K.R. Felzer, A.J. Michael, Improved tests reveal that the accelerating moment release hypothesis is statistically insignificant. J. Geophys. Res. **113**, B08310 (2008). doi:10.1029/2007JB005410
18. C.G. Hatton, I.G. Main, P.G. Meredith, A comparison of seismic and structural measurements of fractal dimension during tensile subcritical crack growth. J. Struct. Geol. **15**, 1485–1495 (1993)
19. A.G. Hawkes, Spectra of some self-exciting and mutually exciting point processes. Biometrika **58**(1), 83–90 (1971)
20. T. Hirata, T. Satoh, K. Ito, Fractal structure of spatial distribution of microfracturing in rock. Geophys. J. Roy. Astr. Soc. **90**, 369–37 (1987)
21. S. Hough, Predicting the Unpredictable: The Tumultuous Science of Earthquake Prediction (Princeton University Press, 2009) p. 272
22. S.C. Jaume, L.R. Sykes, Evolving towards a critical point: a review of accelerating seismic moment/energy release prior to large great earthquakes. Pure Appl. Geophys. **155**, 279–305 (1999)
23. T. Jordan, Y. Chen, P. Gasparini, R. Madariaga, I. Main, W. Marzocchi, G. Papadopoulos, G. Sobolev, K. Yamaoka, J. Zschau, Operational earthquake forecasting: state of knowledge and guidelines for utilization. Ann. Geophys. **54**(4), 361–391 (2011). doi:10.4401/ag-5350
24. H. Kanamori, Earthquake physics and real-time seismology. Nature **451**, 271–273 (2008). doi:10.1038/nature06585
25. F. Kun, I. Varga, S. Lennartz-Sassinek, I.G. Main, Approach to failure in porous granular materials under compression. Phys. Rev. E. **88**, 062207 (2013). doi:10.1103/PhysRevE.88.062207
26. F. Kun, I. Varga, S. Lennartz-Sassinek, I.G. Main, Rupture cascades in a discrete element model of a porous sedimentary rock. Phys. Rev. Lett. **112**, 065501 (2014). doi:10.1103/PhysRevLett.112.065501
27. B. Lawn, *Fracture of Brittle Solids*, 2nd edn. (Cambridge University Press, Cambridge, 1993). p. 371
28. S. Lennartz-Sassinek, I.G. Main, M. Zaiser, C. Graham, Acceleration and localization of subcritical crack growth in a natural composite material. Phys. Rev. E **90**, 052401 (2014). doi:10.1103/PhysRevE.90.052401
29. I.G. Main, A modified Griffith criterion for the evolution of damage with a fractal distribution of crack lengths: application to seismic event rates and b-values. Geophys. J. Int. **107**, 353–362 (1991)
30. I.G. Main, Earthquakes as critical phenomena: Implications for probabilistic seismic hazard analysis. Bull. Seismol. Soc. Am. **85**, 1299–1308 (1995)
31. I. Main, Statistical physics, seismogenesis, and seismic hazard. Rev. Geophys. **34**, 433–462 (1996)
32. I.G. Main, A damage mechanics model for power-law creep and earthquake aftershock and foreshock sequences. Geophys. J. Int. **142**, 151–161 (2000)
33. I.G. Main, L. Li, J. McCloskey, M. Naylor, Effect of the Sumatran mega-earthquake on the global magnitude cut-off and event rate. Nat. Geosci. **1**, p142 (2008)
34. I.G. Main, M. Naylor, Entropy production and self-organized (sub) criticality in earthquake dynamics. Phil. Trans. Roy. Soc. Lond. A **2010**(368), 131–144 (2010). doi:10.1098/rsta.2009.0206

35. I.G. Main, A.F. Bell, P.G. Meredith, S. Geiger, S. Touati, The dilatancy-diffusion hypothesis and earthquake predictability, in *Faulting, Fracturing and Igneous Intrusion in the Earth's Crust*, ed. by D. Healy, R.W.H. Butler, Z.K. Shipton, R.H. Sibson (Geological Society Special Publications, London, 2012), pp. 215–230. doi:10.1144/SP367.15
36. K. Mair, Experimental studies of fault zone development in a porous sandstone, Ph.D. thesis, University of Edinburgh (1997)
37. K. Mair, I.G. Main, S.C. Elphick, Sequential development of deformation bands in the laboratory. J. Struct. Geol. **22**, 25–42 (2000)
38. K. Mair, S. Abe, Breaking up: comminution mechanisms in sheared simulated fault gouge. Pure Appl. Geophys. **168**, 2277–2288 (2011). doi:10.1007/s00024-011-0266-6
39. W. Marzocchi, M. Bebbington, Probabilistic eruption forecasting at short and long time scales. Bull. Volcanol. **74**(8), 1777–1805 (2012)
40. J. McCloskey, S.S. Nalbant, S. Steacy, Indonesian earthquake: earthquake risk from co-seismic stress. Nature **434**, 291 (2005). doi:10.1038/434291a
41. A.P.K.A. Mehta, D.Y. Ben-Zion, Universal mean moment rate profiles of earthquake ruptures. Phys. Rev. E **73**, 056104 (2006)
42. P.G. Meredith, B.K. Atkinson, Stress corrosion and acoustic emission during tensile crack propagation in Whin Sill dolerite and other basic rocks. Geophys. J. Roy. Astron. Soc. **75**, 1–21 (1983). doi:10.1111/j.1365-246X.1983.tb01911.x
43. P.G. Meredith, B.K. Atkinson, Experimental fracture mechanics data for rocks and minerals, in *Fracture Mechanics of Rocks*, ed. by Atkinson B.K (Academic Press, London, 1987). chapter 11
44. G.M. Molchan, T.L. Kronrod, A.K. Nekrasova, Immediate foreshocks: time variation of the b-value. Phys. Earth Planet. Inter. **111**(3–4), 229–240 (1999). doi:10.1016/S0031-9201(98)00163-0
45. M. Naylor, J. Greenhough, J. McCloskey, A.F. Bell, I.G. Main, Statistical evaluation of characteristic earthquakes in the frequency-magnitude distributions of Sumatra and other subduction zone regions. Geophys. Res. Lett. **36**, L20303 (2009). doi:10.1029/2009GL040460
46. H. Nechad, A. Helmstetter, R. El Guerjouma, D. Sornette, Andrade and critical time-to-failure laws in fiber-matrix composites: experiments and model. J. Mech. Phys. Solids **53**(5), 1099–1127 (2005)
47. Z. Olami, H.J.S. Feder, K. Christensen, Self-organized criticality in a continuous, nonconservative cellular automaton modeling earthquakes. Phys. Rev. Lett. **68**, 1244 (1992)
48. I.O. Ojala, I.G. Main, B.T. Ngwenya, Strain rate and temperature dependence of Omori law scaling constants of AE data: implications for earthquake foreshock-aftershock sequences. Geophys. Res. Lett. **31**, L24617 (2004). doi:10.1029/2004GL020781
49. Y. Ogata, Statistical models for earthquake occurrences and residual analysis for point processes. J. Am. Stat. Assoc. **83**, 9–27 (1988)
50. M.D. Petersen, T. Cao, K.W. Campbell, A.D. Frankel, Time-independent and time-dependent seismic hazard assessment for the state of California: uniform California earthquake rupture forecast model 1.0. Seismol. Res. Lett. **78**, 99–109 (2007)
51. J. Rundle, E. Preston, S. McGinnis, W. Klein, Why earthquakes stop: growth and arrest in stochastic fields. Phys. Rev. Lett. **80**, 5698 (1998)
52. J.B. Rundle, W. Klein, Nonclassical nucleation and growth of cohesive tensile cracks. Phys. Rev. Lett. **63**, 171 (1989)
53. E.K.H. Salje, K.A. Dahmen, Crackling noise in disordered materials. Ann. Rev. Condens. Matter Phys. **5**, 233–254 (2014). doi:10.1146/annurev-conmatphys-031113-133838
54. P.R. Sammonds, P.G. Meredith, I.G. Main, Role of pore fluids in the generation of seismic precursors to shear fracture. Nature **359**, 228–230 (1992)
55. C. Saouridis, J. Mazars, Prediction of the failure and size effect in concrete via a bi-scale damage approach. Eng. Comput. **9**, 329–344 (1992)
56. D.R. Scott, Seismicity and stress rotation in a granular model of the brittle crust. Nature **381**, 592–595 (1996). doi:10.1038/381592a0

57. J.P. Sethna, K.A. Dahmen, C.R. Myers, Crackling noise. Nature **410**, 242–250 (2001). doi:10.1038/35065675
58. D. Sornette, G. Ouillon, Dragon-kings: mechanisms, statistical methods and empirical evidence. Eur. Phys. J. Spec. Top. **205**, 1–26 (2012)
59. D. Spasojevic, S. Bukvi, S. Miloevi, H.E. Stanley, Barkhausen noise: elementary signals, power laws, and scaling relations. Phys. Rev. E **54**, 2531–2546 (1996)
60. S. Touati, M. Naylor, I.G. Main, The origin and non-universality of the earthquake inter-event time distribution. Phys. Rev. Lett. **102**, 168501 (2009). doi:10.1103/PhysRevLett.102.168501
61. Turcotte, D.L., Fractals and chaos in geology and geophysics. (Cambridge, 1992), p. 221
62. J. Vasseur, F.B. Wadsworth, Y. Lavallée, A.F. Bell, I.G. Main, D.B. Dingwell, Heterogeneity: the key to failure forecasting. Sci. Rep. **5**, 13259 (2015). doi:10.1038/srep13259
63. M. Wyss (ed.), *Evaluation of Proposed Earthquake Precursors* (American Geophysical Union, Washington, DC, 1991). 94 pp
64. G. Yakovlev, J.B. Rundle, R. Shcherbakov, D.L. Turcotte, Inter-arrival time distribution for the non-homogeneous Poisson process. (Elsevier Science, 2005), http://arXiv.org/abs/cond-mat/0507657
65. L. Zhang, E.K.H. Salje, X. Ding, J. Sun, Strain-rate dependence of twinning avalanches at high speed impact. Appl. Phys. Lett. **104**, 162906 (2014)